

R.I.P. : A Simple Black-box Attack on Continual Test-time Adaptation

Trung-Hieu Hoang¹ Duc Minh Vo² Minh N. Do¹

¹Department of Electrical and Computer Engineering, University of Illinois at Urbana-Champaign, USA

²The University of Tokyo, Japan

{hthieu, minhdo}@illinois.edu,

vmduc@nlab.ci.i.u-tokyo.ac.jp

Abstract

Test-time adaptation (TTA) has emerged as a promising solution to tackle the continual domain shift in machine learning by allowing model parameters to change at test time, via self-supervised learning on unlabeled testing data. At the same time, it unfortunately opens the door to unforeseen vulnerabilities for degradation over time. Through a simple theoretical continual TTA model, we successfully identify a risk in the sampling process of testing data that could easily degrade the performance of a continual TTA model. We name this risk as **Reusing of Incorrect Prediction (RIP)** that TTA attackers can employ or as a result of the unintended query from general TTA users. The risk posed by RIP is also highly realistic, as it does not require prior knowledge of model parameters or modification of testing samples. This simple requirement makes RIP as the first **black-box** TTA attack algorithm that stands out from existing white-box attempts. We extensively benchmark the performance of the most recent continual TTA approaches when facing the RIP attack, providing insights on its success, and laying out potential roadmaps that could enhance the resilience of future continual TTA systems.

1. Introduction

“No man ever steps in the same river twice, for it’s not the same river and he’s not the same man”.

– Heraclitus (535 B.C. to 475 B.C.) –

This age-old statement holds in modern machine learning (ML) research, where the real-world environment, like a river, is constantly changing, necessitating adaptation to continual domain shifts [7, 18, 41]. Recently recognized continual *Test-Time Adaptation (TTA)* [48, 49] is a powerful tool for addressing this need by allowing the model parameters to change at the test time. Nonetheless, much like the man who is no longer the same after stepping into the river, it is uncertain whether the adapted model will evolve in a better or worse direction. For instance, under extended time

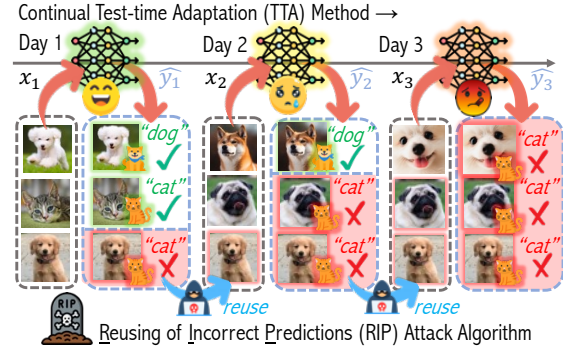


Figure 1. An illustration of our **Reusing of Incorrect Predictions (RIP)** attack against a continual test-time adaptation (TTA) method. Here the attacker intentionally reuses samples that were incorrectly predicted in the subsequent rounds to make the model more confident in these erroneous predictions. RIP is the first black-box attack that can realistically collapse a TTA model.

horizons [17, 40] or challenging testing streams [8, 43, 53], recent studies raise a critical concern that TTA models *can be collapsed*, resulting in predictions that are confined to a single set of categories regardless of the input after several iterations. As such, unforeseen risks are inevitable in TTA. Deepening the understanding of these risks, including how they occur and how to prevent them, is crucial for ensuring a reliable, and trustworthy real-world TTA deployment.

While some risks may naturally arise during a TTA process [17, 40, 43, 53], we delve into a more perilous situation where such systems are particularly vulnerable to malicious samples, which attackers could exploit to degrade the performance of a system intentionally. This threat is known as *adversarial model attack* [9, 45, 50]. To our best knowledge, only a limited number of prior studies investigated this threat on continual TTA models [2, 39, 51]. Unfortunately, all resort to the white-box setting (assuming access to parameters of a victim model), which is impractical to implement. The gap here urges us to extend the concept of *black-box* [12, 38] attack to continual TTA that is not only more realistic but also a pioneering work in this area.

TTA updates a ML model using testing samples available at test time. Thus, an attack algorithm functions by modify-

ing that batch of testing samples [2, 39, 51]. Theoretically speaking, the sampling process is manipulated. We aim to find a simple yet dangerous sampling operator, opening the ability to attack a TTA method effortlessly. By extending Gaussian Mixture Model Classifier (GMMC) [17], a handy theoretical model for understanding TTA, we first discover one such sampling strategy that can easily fool TTA to converge undesirably, under a condition. This condition is not hard to meet in almost every modern continual TTA methods [6, 17, 49, 53] that requires a random image transformation [42] to be applied during training at test time. The idea behind augmentation is straightforward, based on the fact that the semantics of an image are unchanged under mild random image transformations. These augmentation strategies generate more samples that favor the adaptation efficacy [16, 27, 55]. Yet, this good practice becomes problematic when incorrectly predicted samples are augmented and used for adaptation. Ultimately, it turns into the “*Achilles’ heel*”¹ of TTA that one can exploit to attack, even within the *black-box* constraints. Aside from the attack scenario, the discussion here is still relevant if a general user unintentionally queries samples that fall into this *corner test case*.

This leads us to develop **Reusing of Incorrect Predictions (RIP)**, the first **black-box** attack algorithm to make a TTA model prone to collapse. RIP is illustrated by a simple binary classification task in Fig. 1. Here, the attacker intentionally picks incorrect predictions in previous TTA steps (highlighted in red) and reuses them in the subsequent testing batches. With random augmentation applied, incorrectly predicted samples and their augmented variants are used for TTA. We discover that under RIP, the decision boundary of a victim class is erroneously shifted, penetrated, and dominated by nearby classes. Over time, a TTA model can be collapsed in this way. Undoubtedly, RIP is a straightforward attack algorithm that does not require any specialized expertise. The contributions of this work are:

- Through a theoretical model, we *discovered a threat* in which data augmentation in TTA and *i.i.d.* sampling assumption violation can make a model collapse (Sec. 3).
 - Inspired by this observation, *Reusing of Incorrect Predictions (RIP)* - the first black-box attack algorithm targeting continual TTA methods is proposed (Sec. 4).
 - Through extensive experiments, we *confirm the vulnerability* of many recent continual TTA methods (Sec. 5).
 - A series of ablation studies *verifies the root causes* of vulnerability that can help to mitigate RIP attack (Sec. 6).
- Visit the Appendix for a summary of the related work.

2. The Continual TTA Procedure

This section presents the major notations and describes key components living in a continual TTA method.

¹An idiom from *Greek mythology* that refers to a weakness of a system or person that can lead to failure, despite the supreme overall strength.

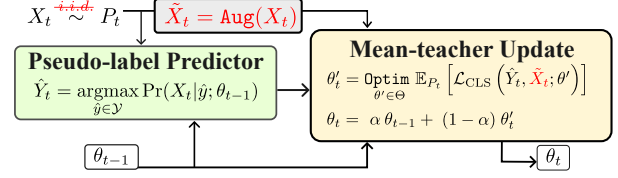


Figure 2. The key operational steps of a continual TTA method. We extend the model in [17] (red highlighted) with the augmentation operator $\text{Aug}(\cdot)$ and investigate its effect in a vulnerable scenario where testing samples are *not i.i.d.* sampled from a distribution P_t , but instead selectively sampled to collapse a model.

2.1. Continual Test-time Adaptation

Notations. We focus on a ML classifier $f_t : \mathcal{X} \rightarrow \mathcal{Y}$, parameterized by $\theta_t \in \Theta$ (parameter space) that maps an input image $x \in \mathcal{X}$ to a class-label $y \in \mathcal{Y}$. A TTA method continuously modifies f_t at each time step $t \in \mathcal{T}$. Let the capital letters $(X_t, Y_t) \in \mathcal{X} \times \mathcal{Y}$ denote a pair of *random variables* with the joint distribution $P_t(x, y) \in \mathcal{P}_d, t \in \mathcal{T}$. In practice, X_t is in the form of a batch of B testing samples. The superscript such as $X_t^{(i)}$ is used to denote the i -th realization of a random variable, when necessary. The covariate shift [41] is assumed: $P_t(x)$ and $P_{t'}(x)$ could be different but $P_t(y|x) = P_{t'}(y|x)$ holds $\forall t \neq t'$. At $t = 0$, θ_0 is a source model trained on labeled data from distribution P_0 .

The Continual TTA Procedure. At $t > 0$, the continual TTA process follows the diagram provided in Fig. 2:

- X_t is sampled from distribution P_t . While *i.i.d.* sampling is typically assumed, this work discusses a critical point: “*What if this assumption fails to hold?*”
- The pseudo-label predictor (Sec. 2.4) guesses the label for X_t based on θ_{t-1} (from the previous step):

$$\hat{Y}_t = f_{t-1}(X_t). \quad (1)$$

- Besides returning \hat{Y}_t (Eq. 1) as a prediction, pseudo-labels are used for minimizing an objective function (Sec. 2.2), adapting itself $f_{t-1} \rightarrow f_t$ (Sec. 2.3).

2.2. Loss Functions

With only unlabeled data (X_t) available at test time, a *pseudo label* [22] (\hat{Y}_t as in Eq. 1) is introduced for each X_t . As a shorthand notation, we omit t and denote the following *probability vectors* \mathbf{p} and \mathbf{q} . Here, $p_{\hat{y}} = \Pr\{\hat{Y}_t = \hat{y}\}$ and $q_{\hat{y}} = \Pr\{f_t(X_t) = \hat{y}\}$, for $\hat{y} \in \mathcal{Y}$ represent the conditional probability of the pseudo-label predictor and the model assign label \hat{y} for a given input sample (i.e., the intermediate model output after softmax and before argmax). Existing loss functions in the field can be classified into two groups: **Augmenting-free Loss Functions:** In the most basic form, pioneering studies [34, 48] adopt the *Entropy (Ent)* loss:

$$\mathcal{L}_{\text{Ent}}(\mathbf{q}) = - \sum_{\hat{y} \in \mathcal{Y}} q_{\hat{y}} \log(q_{\hat{y}}). \quad (2)$$

Utilizing the pseudo-label, the *Cross Entropy* (CE) [11] loss replaces \mathbf{p} in the position of one \mathbf{q} in Eq. 2:

$$\mathcal{L}_{\text{CE}}(\mathbf{p}, \mathbf{q}) = - \sum_{\hat{y} \in \mathcal{Y}} p_{\hat{y}} \log(q_{\hat{y}}), \quad (3)$$

While there are two replacement choices, a symmetric version - *Symmetry Cross Entropy* (SCE) loss [30]:

$$\mathcal{L}_{\text{SCE}}(\mathbf{p}, \mathbf{q}) = - \frac{1}{2} \left(\sum_{\hat{y} \in \mathcal{Y}} p_{\hat{y}} \log q_{\hat{y}} + q_{\hat{y}} \log p_{\hat{y}} \right)$$

is also commonly used. In RMT [6], an elaborated version that applies \mathcal{L}_{SCE} twice is used as their self-training loss (\mathcal{L}_{RMT}). To improve adaptation stability [30], the *Soft Likelihood Ratio* (SLR) loss [31] modifies CE as follows:

$$\mathcal{L}_{\text{SLR}}(\mathbf{p}, \mathbf{q}) = -w \sum_{\hat{y} \in \mathcal{Y}} p_{\hat{y}} \log \left(\frac{q_{\hat{y}}}{\sum_{\hat{y}' \neq \hat{y}} q_{\hat{y}'}} \right), \quad (4)$$

with w is the corresponding weight for sample \hat{y} .

Augmenting Loss Functions: Later studies [6, 30, 33, 43, 49, 53] further advance TTA with the use of augmented samples. With Aug is a random data augmentation operator, instead of using \mathbf{q} (e.g., in \mathcal{L}_{CE} - Eq. 3), $\tilde{\mathbf{q}}$ is used with:

$$\tilde{q}_{\hat{y}} = \Pr\{f_t(\tilde{X}_t) = \hat{y}\}; \quad \tilde{X}_t = \text{Aug}(X_t). \quad (5)$$

Here, $\text{Aug}(X_t)$ replaces X_t . The consistency of the model output given X_t and its diverse views \tilde{X}_t , via random augmentation, is encouraged to increase TTA update efficacy.

2.3. Model Update

TTA with Mean Teacher Update. To achieve a stable optimization process, the main (*teacher*) model f_t are updated indirectly through a *student* model f'_t with parameter θ'_t [6, 8, 46, 48, 53]. With \mathcal{L}_{CLS} as a placeholder for the loss function (Sec. 2.2), and a regularizer \mathcal{R} , the student model (f'_t) is first updated with a generic optimization operator Optim , followed by an *Exponential Moving Average* (EMA) update of the teacher model parameter θ_{t-1} :

$$\theta'_t = \underset{\theta' \in \Theta}{\text{Optim}} \mathbb{E}_{P_t} \left[\mathcal{L}_{\text{CLS}}(\hat{Y}_t, X_t; \theta') \right] + \lambda \mathcal{R}(\theta'), \quad (6)$$

$$\theta_t = \alpha \theta_{t-1} + (1 - \alpha) \theta'_t, \quad (7)$$

with $\alpha \in (0, 1)$ - the EMA update rate, and $\lambda \in \mathbb{R}^+$ - the coefficient of the regularization term are hyper-parameters.

Source Model Weights Ensemble Update: Suggested in ROID [30] to avoid self-training and mean teacher update [46]. The accumulated model is updated via:

$$\theta_t = \alpha \theta_0 + (1 - \alpha) \theta'_t, \quad (8)$$

with θ_0 is the parameter of the source model.

2.4. Pseudo-label Predictor

The pseudo-label of augmented samples (\hat{y}_t) in Eq. 5 can be predicted in two ways. Let denote \tilde{f}_t be the model updated

with EMA in Eq. 7 (teacher model). We have:

- **Pseudo-labels from Teacher Model:** The earliest work - CoTTA [49] proposes the following strategy:

$$\hat{y}_t = \tilde{f}_{t-1}(\tilde{x}_t). \quad (9)$$

- **Pseudo-labels from Student Model:** This strategy is used in almost every follow-up study after CoTTA, (e.g., RMT [6], ROID [30], RoTTA [53] or TRIBE [43]):

$$\hat{y}_t = f_{t-1}(\tilde{x}_t). \quad (10)$$

3. A Risk in TTA with Data Augmentation

By inspecting a toy example of a simple theoretical model (Sec. 3.1), this section delves into our first findings on a sampling strategy, namely *Incorrectly Prediction Sampling* (IPS) (Sec. 3.2) that negatively impacts a TTA method.

3.1. Augmented Gaussian Mixture Model Classifier

In [17], Hoang *et al.* introduces a simple yet representative Gaussian Mixture Model Classifier (GMMC) that replicates the behavior of a real-world continual TTA model for a theoretical analysis. However, *GMMC fails to account for the role of the random image augmentation operator*, a common practice in modern continual TTA. This study extends GMMC along this line and introduces an inspection, shedding light on the introduction of our attack algorithm.

To replicate the Aug operator in Eq. 5 on GMMC, we employ *Additive White Gaussian Noise* (AWGN) that can be directly applied to the data used for optimizing GMMC:

$$\tilde{X}_t = \text{Aug}_{\sigma}(X_t) = X_t + \delta, \quad \delta \sim \mathcal{N}(0, \sigma). \quad (11)$$

The level of data augmentation can be controlled by σ . A larger value of σ corresponds to a stronger augmentation scheme, and $\sigma = 0$ means no data augmentation is applied.

While AWGN is relatively simple, Fig. 3 empirically justifies its validity as a *proxy for image-based operators* Aug . In Fig. 3-(left), the 2D *t-SNE* [47] projects deep-feature embedding (source model) of 100 random CIFAR-10-C [14] images from two classes. Five augmented variations (using common augmentation operators - see the Appendix) are visualized together with the original images. Data augmentation expands the coverage of a sample into multiple directions around their initial data points (similar to findings in [28, 54]). This effect is highly analogous to the one introduced by AWGN on 1-dimensional data used in GMMC. In sum, GMMC with AWGN in Eq. 11 *can potentially serve as a surrogate model for analyzing a TTA model with image-augmentation operator* introduced in Eq. 5.

3.2. Incorrect Prediction Sampling on GMMC

The Shifting-Boundary Effect. Since random augmentation can generate variations around an original sample, the optimal decision boundary optimized on a combination of

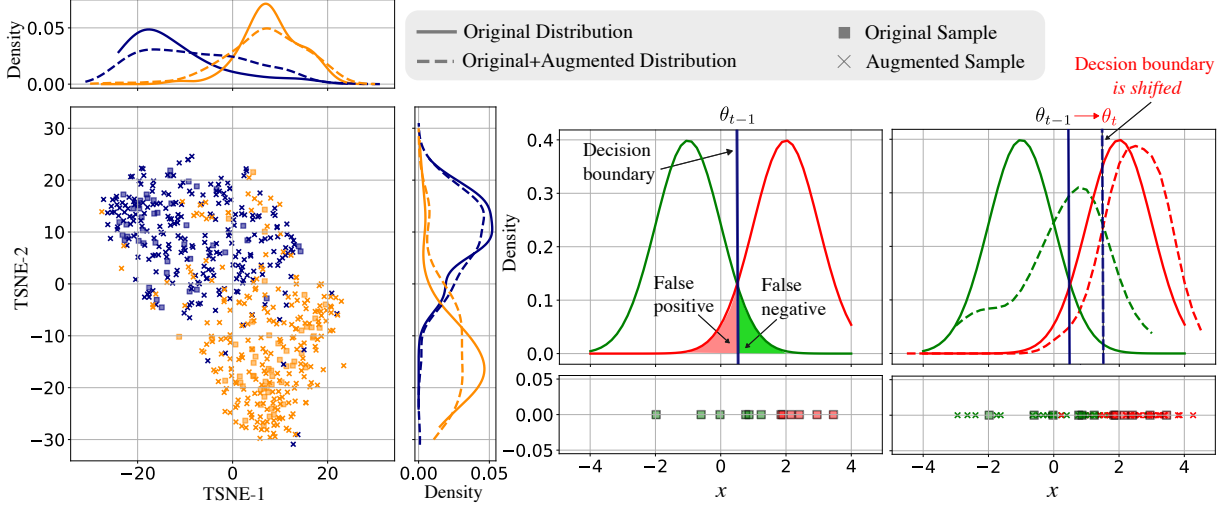


Figure 3. The similarity in the effect of random data augmentation on images of CIFAR-10-C [14] and synthetic data used in Gaussian Mixture Model Classifier (GMMC). (left) 2D t -SNE [47] projection of the deep feature vectors of real images. (middle) Samples drawn from two Gaussian distributions and the best theoretical separation boundary on GMMC (solid line). Regions with incorrect predictions are highlighted. (right) An Additive White Gaussian Noise (AWGN) generates augmented samples for GMMC and the decision boundary separates original and augmented samples (dashed line). The shifting of decision boundaries when training with augmented samples is similarly observed on both real images and GMMC simulated data, allowing our analysis to focus on GMMC+AWGN for their simplicity.

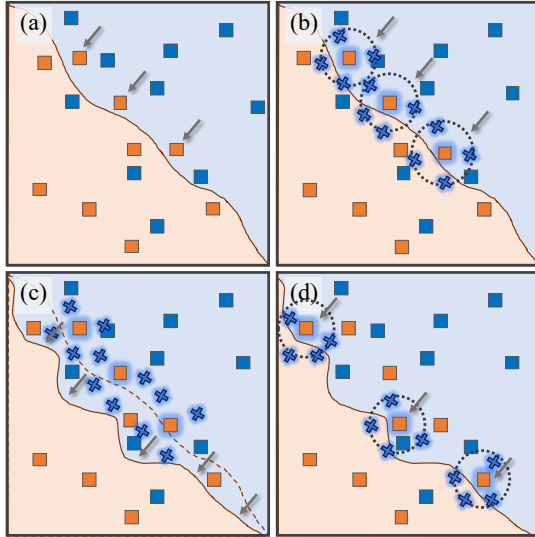


Figure 4. A step-by-step illustration of the shifting-boundary effect caused by incorrect prediction sampling (IPS), elaborating on Fig. 3-left. Arrows serve as pointers. (a) Mispredicted samples from a victim class (orange) are sampled for TTA. (b) Randomly augmented variations (denoted by \times) are generated, expanding the area (dashed circles) around the original samples. (c) The updated decision boundary expands to cover these samples - highlighted with the blue halo effect, penetrating the victim class. (d) The process repeats, reducing the chance of predicting the victim class.

augmented and original samples *can be shifted* as shown in Fig. 3-right. It is noted that the distribution of the original did not change, and augmented samples near the decision boundary make this drift. Finding samples in this area

is straightforward as they are likely to be incorrectly predicted, either false positives or negatives (Fig. 3-middle).

Incorrect Prediction Sampling (IPS). The shifting boundary effect gives an idea of a *sampling operator* that X_t is only selected if it comes from a victim class (y_a) and its pseudo-label is incorrectly predicted (i.e., $\hat{Y}_t \neq Y_t \wedge Y_t = y_a$). We name this strategy as *IPS*. When X_t 's are not *i.i.d.* sampled from P_t , but IPS operator is applied instead, an attacker can easily modify the decision boundary of a TTA model. Fig. 4 illustrates the shifting boundary effect caused by IPS. Due to the expansion of incorrect predictions of the victim class via augmentation and TTA model update, its decision boundary is penetrated by the nearby classes.

Numerical Simulation. To empirically confirm the case of IPS and Aug on GMMC, we carry out a numerical simulation in Fig. 5, with $T = 120$ adaptation steps (See the Appendix for setup details). The collapse is observed when most predictions converge to a single label, no matter what the input data is (see Def. 1). In Fig. 5a, the model is collapsed when IPS is applied while this is not the case in Fig. 5b. When removing Aug in Fig. 5c, the boundary can be shifted, but a total collapse is not observed. In sum, the collapse only happens when the *two conditions are met*: IPS is performed and Aug operator is in place. Slowing down the update α (Eq. 7) helps mitigate the effect of RIP (Fig. 5d). We will return back to this discussion in Sec. 6.5.

4. Reusing Incorrect Predictions (RIP) Attack

Inspired by IPS, this section establishes the threat model and our RIP attack, an algorithm introducing this threat.

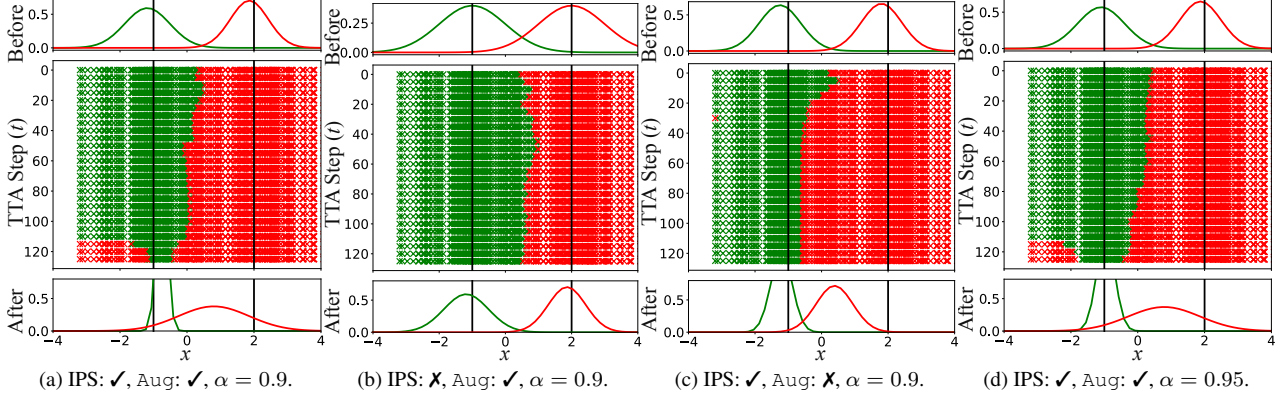


Figure 5. Simulation results on the Gaussian Mixture Model Classifier (GMMC) representing the effect of Incorrect Prediction Sampling (IPS), augmentation operator (Aug), and update rate (α). (✓) denotes if the operator is enabled, and (✗) vice versa. The distribution before (top) and after adaptation (bottom) is visualized. The (middle) plot shows the shifting in model prediction (on the same set of samples) after every 20 steps. (a)-(c) GMMC is collapsed if IPS and Aug are simultaneously enabled. (d) Increasing α partially mitigates the collapse.

Attack Type	Attack Objective		Attack Algorithm	Model Parameters	Benign Sample	Source Dataset
White-box	Targeted	Flipping the prediction of a victim category (class) to a target category	TePA [2]	✓	✓	✓
	Stealthy Targeted	Achieving the above objective while maintaining the performance in other categories	DIA [51]	✓	✓	✗
	Indiscriminate	Degrading the performance of all categories				
Black-box (ours)	Collapsing (ours)	Degrading the performance of at least one (or more) category	RIP (ours)	✗	✗	✗

Table 1. A comparison of existing white-box TTA attack attempts in [2, 51] and **RIP**-our proposed **black-box** attack algorithm that makes a TTA model **collapse**. A summary of the main attack objectives and the representative attack algorithms are provided. For each algorithm, we highlight whether an assumption is necessary (✓) or not (✗) for a success attack. The assumptions are: (Model Parameters) - accessing model parameters at any time, either before (source model) or after an adaptation step; (Benign Sample) - intercepting and pixel-level modifying benign samples from other users to generate malicious samples; (Source Dataset) - accessing or sampling from the distribution that creates the source dataset. Although the attack goal is weaker than the ones in the white-box attack, our *collapsing attack* is still considered dangerous in practice. This goal is realized by RIP - an attack algorithm that lifts all assumptions made by previous attempts.

4.1. Threat Model

The threat model in this study focuses on two main aspects: first, making a TTA *model collapsed* as the main objective and second, *black-box* as the constraint for the attack.

Collapsing Attack Objective. *Collapsing attack on continual TTA is first introduced in this study.* Its primary objective is to make a continual TTA model that tends to *ignore* some categories in $\tilde{\mathcal{Y}} \subset \mathcal{Y}$. This is called model collapse, and Definition 1 restates its mathematical definition in [17]:

Definition 1 (Model Collapse). *A model is said to be collapsed from step $\tau \in \mathcal{T}, \tau < \infty$ if there exists a non-empty subset of categories $\tilde{\mathcal{Y}} \subset \mathcal{Y}$ such that $\Pr\{Y_t \in \tilde{\mathcal{Y}}\} > 0$ but the marginal $\Pr\{\hat{Y}_t \in \tilde{\mathcal{Y}}\}$ converges to zero in probability:*

$$\lim_{t \rightarrow \tau} \Pr\{\hat{Y}_t \in \tilde{\mathcal{Y}}\} = 0.$$

As it is irrecoverable once collapsed, the only remedy would be resetting all parameters back to θ_0 . Tab. 1 compares the existing continual TTA attack objectives [51] and

our TTA model collapsing TTA attack (columns 2-3).

Metric for Collapsing Attack. We simply compute the average class-wise testing error among all categories and report the increment versus the same model without attack.

Black-box Continual TTA Model Attack. In a TTA black-box attack, an attacker can only interact with queries and model responses [38]. Before and during the adaptation, accessing the model architecture and parameters, the operating TTA algorithm, gradient information, optimizer state, etc., or queries from other users are strictly forbidden at any time. We define the terminology of *black-box TTA attack* as any attack algorithm following these constraints.

4.2. Reusing Incorrect Prediction Attack Algorithm

Attack Description. The idea of *Reusing Incorrect Prediction (RIP)* is as simple as IPS. RIP capitalizes on the vulnerability of TTA in Sec. 3 by intentionally reusing incorrect predictions from one victim class y_a in subsequent adaptation steps. All mispredicted samples from y_a in the previous steps are accumulated and reused. A severe do-

Algorithm 1 Reusing Incorrect Predictions (RIP) Attack

Input: Labeled dataset \mathcal{D}_a for attack, victim attack class y_a , victim continual TTA model $f_t(x)$, testing batch size B , the number of attack rounds T_a .

// Initialize \mathcal{S}_0 with samples in \mathcal{D}_a

```
1  $\mathcal{S}_0 \leftarrow \left\{ \left( X_0^{(i)}, Y_0^{(i)} \right) \sim \mathcal{D}_a \right\}_{i=1}^B$ 
2 for  $t \in [1, \dots, T_a]$  do
    // Predictions from TTA model
3    $\hat{Y}_{t-1}^{(i)} \leftarrow f_{t-1} \left( X_{t-1}^{(i)} \right), X_t^{(i)} \in \mathcal{S}_{t-1}$ 
    // Set of incorrect predictions
4    $\mathcal{I}_t \leftarrow \left\{ X_t^{(i)} | Y_t^{(i)} \neq \hat{Y}_{t-1}^{(i)} \wedge Y_t^{(i)} = y_a, i = 1 \dots B \right\}$ 
    // Fulfilling with samples from  $\mathcal{D}_a$ 
5    $\mathcal{S}_t \leftarrow \mathcal{I}_t \cup \left\{ \left( X_t^{(i)}, Y_t^{(i)} \right) \sim \mathcal{D}_a \right\}_{i=1}^{B-|\mathcal{I}_t|}$ 
6 end
```

main shift and the imperfection of f_{t-1} under this new distribution make the pseudo-label in Eq. 1 erroneous. Hence, finding incorrect predictions is convenient. The only requirement here for RIP is that the attacker has access to a labeled dataset (\mathcal{D}_a) that is reasonably large to find at most B incorrect predictions. *RIP strictly follows the black-box setting* and does not add any specific or unusual setup that favors the attackers over the victim’s continual TTA model. Alg. 1 gives the pseudo-code and Fig. 1 provides a graphical illustration of our RIP attack algorithm in a simple case.

4.3. Comparison to Prior TTA Attack Studies

Black-box versus White-Box Attack. White-box continual TTA attacks assume the adversary has complete knowledge of the underlying TTA model. Poisoning [2] or distribution invading [39, 51] attacks (DIA) fall into this category, where the source model (or the one before adaptation) is used as a surrogate model for generating adversarial attack samples. Simply studying the developer manual of a popular ML API, for instance, ones from Open AI², the white-box attack is obviously unrealistic to implement. Most recent APIs *do not reveal the source model or dataset it was trained on to general users*. Hence, a black-box attack is the only possibility. Tab. 1 summarizes a comparison between white- and black-box algorithms (columns 4-7).

RIP versus Other Attack Algorithms. RIP is the first black-box attack attempt that stands out from existing ones. We note that previous algorithms generate adversarial samples by directly adding pixel-level perturbations to the original images. While these subtle changes may be *imperceptible to humans*, a trained adversarial detector can identify and reject malicious samples [1, 23, 36, 50] generated.

²<https://platform.openai.com/docs/api-reference>

5. Continual TTA Methods Under RIP Attack

5.1. Experimental Setup

Continual TTA Task, Dataset and Methods. The effect of RIP attack is evaluated on the image classification task, with three benchmarks including CIFAR10 \rightarrow CIFAR10-C, CIFAR100 \rightarrow CIFAR100-C, and ImageNet \rightarrow ImageNet-C [14]. The following continual TTA methods (f_t in Alg. 1) are studied: CoTTA [49], EATA [34], RMT [6], RoTTA [53], ROID [30], TRIBE [43], and PeTTA [17].

Attack Scenario. We employ RIP attack follows Alg. 1, with $T_a = 500$ rounds, $B = 64$ and \mathcal{D}_a is a set of images corrupted by impulse noise from each dataset. The choice of corruption here is arbitrary and B follows prior studies. Results in the Appendix show that other options also perform well. In following experiments, we compute the error of each class independently, after every 25 adaptation step, and report the average value among all classes. For a robust estimation, we repeat the attack 10 times (trials), each with a different victim attack label y_a , randomly selected and averaged across trials. For all compared TTA methods, we use the default set of hyper-parameters from their authors.

5.2. Vulnerability of Existing TTA Methods

The vulnerability of many existing TTA methods under RIP attack is confirmed in Tab. 2. *Overall, the average testing error increment is observed in all datasets*. To qualitatively observe this effect on CIFAR-10-C [14], we visualize the testing error after every 25 steps. Two scenarios are considered: under RIP attack (Fig. 6a), and no attack (Fig. 6b). Surprisingly, CoTTA [49] or EATA [34] - the earliest methods have the best resilience to RIP. The following Sec. 6 conducts ablation studies to explain when a TTA method fails or thrives. As a teaser for their resilience, EATA does not involve training with augmented sample Aug , CoTTA is a simple method that uses the teacher model for predicting the pseudo-labels (Eq. 9). However, we note that while their limitations and assumptions do exist, motivating the development of many subsequent methods [8, 53]. *The behavior of real TTA methods matches the risk* (Sec. 3). Additional attack results are provided in the Appendix.

6. Analyzing the Causes of Vulnerability

There are multiple living components inside a continual TTA. This section introduces a baseline method (Sec. 6.1) and a series of ablation studies, isolating those factors to evaluate the risk of existing design choices: loss function (Sec. 6.2), level of augmentation (Sec. 6.3), pseudo-label generator (Sec. 6.4) and model update scheme (Sec. 6.5).

6.1. Baseline Continual TTA Method

We employ a baseline continual TTA method based on Eq. 5, 7, closed to CoTTA [49]. This simple model updates

Method	Venue	CIFAR-10-C		CIFAR-100-C		ImageNet-C	
		No Attack	RIP Attack	No Attack	RIP Attack	No Attack	RIP Attack
No TTA	-	0.7292	0.7292(↑ 0%)	0.3937	0.3937(↑ 0%)	0.8155	0.8155(↑ 0%)
PeTTA [17]	NeurIPS'24	0.3385	0.4704(↑ 39%)	0.3634	0.4617(↑ 27%)	0.7439	0.8174(↑ 10%)
RoTTA [53]	CVPR'23	0.4492	0.5872(↑ 31%)	0.3751	0.5354(↑ 43%)	0.8105	0.8237(↑ 2%)
ROID [30]	WACV'24	0.2836	0.3719(↑ 31%)	0.2885	0.4729(↑ 64%)	0.7061	0.7536(↑ 7%)
TRIBE [43]	AAAI'24	0.4537	0.5502(↑ 21%)	0.3608	0.5691(↑ 58%)	0.7737	0.7978(↑ 3%)
CoTTA [49]	CVPR'22	0.3105	0.3417(↑ 10%)	0.4262	0.4383(↑ 3%)	0.7524	0.7593(↑ 1%)
RMT [6]	CVPR'23	0.2871	0.3502(↑ 22%)	0.3371	0.4155(↑ 23%)	0.7182	0.7496(↑ 4%)
EATA [34]	ICML'22	0.2952	0.3488(↑ 18%)	0.2926	0.4251(↑ 45%)	0.7568	0.7571(↑ 0%)

Table 2. Average of the class-wise testing error (lower is better) across 500 adaptation steps and 10 RIP attack trials of the studied TTA methods [6, 17, 30, 34, 43, 49, 53]. The performance of the source model (No TTA) and the TTA method without RIP attack (No Attack) are included for comparison. While the damage caused by RIP may vary across algorithms, most state-of-the-art continual TTA approaches are severely affected. The number in brackets shows the percentage increase in testing error under the RIP attack compared to no attack.

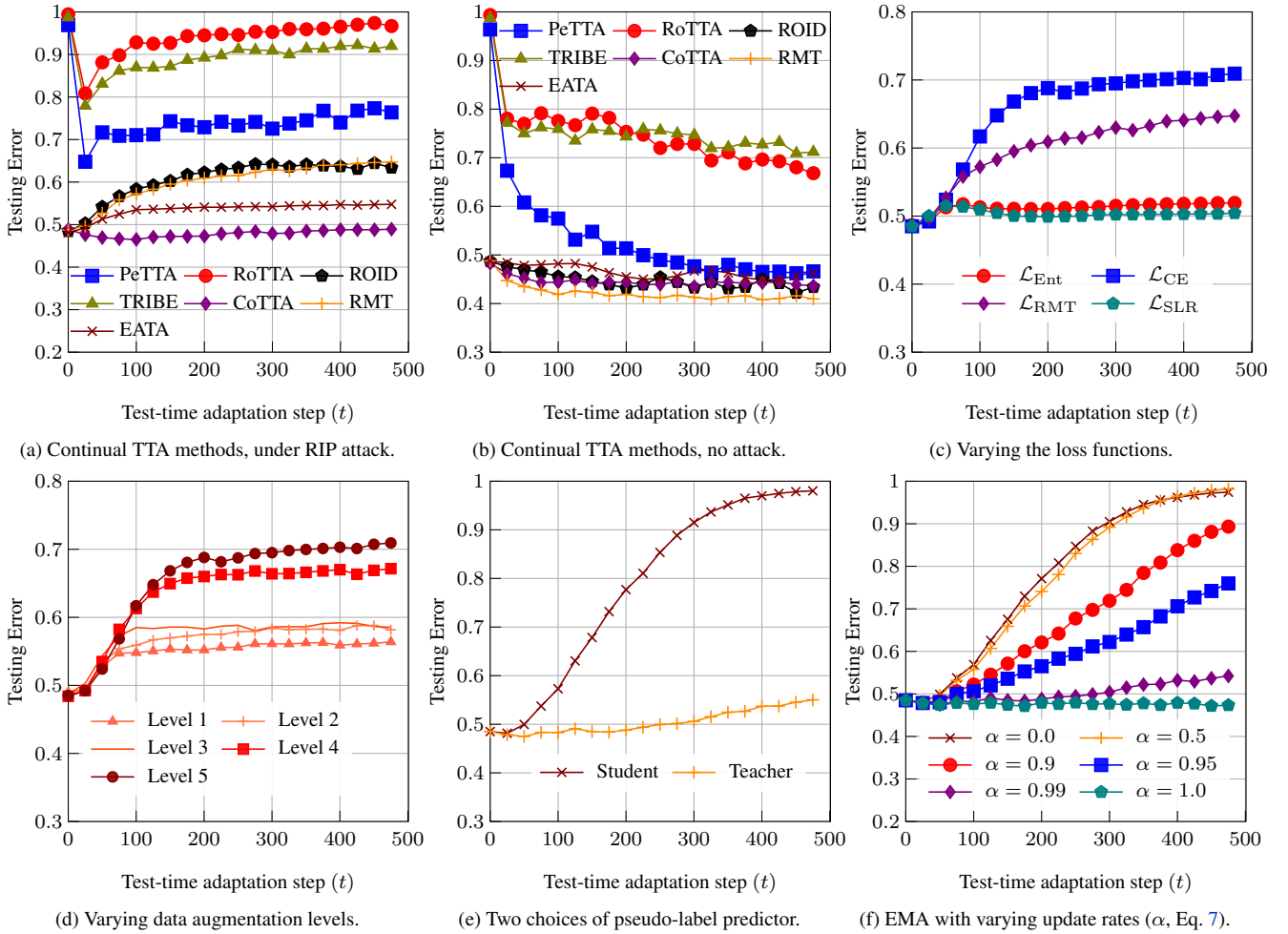


Figure 6. Average of the worst category-wise testing error in various CIFAR-10-C [14] experiments. (a) The testing error of several major TTA algorithms [6, 30, 43, 53] progressively raises under RIP attack while some early-generation algorithms [34, 49] persist, surprisingly. (b) This was not the case with no attack (normal condition). Ablation studies on a baseline model, trained with \mathcal{L}_{CE} (with augmentation) and update rate $\alpha = 0.99$ are conducted. The plot (c) confirms the risk of RIP attack on TTA methods using data augmentation in their loss function, (d) the stronger the augmentation, the more vulnerable. (e) Using mean-teacher (EMA) model update, or (f) slowing down the update rate can mitigate the effect (compared to $\alpha = 0$, no EMA update), but fail to eliminate it (considering $\alpha = 1$, no TTA).

the linear parameters of batch normalization [19, 48]. For simplicity, the ablation studies are conducted on CIFAR-10-C [14] - 10 trials averaged. Without specifically noted, the \mathcal{L}_{CE} with augmentation and update rate $\alpha = 0.99$ are used.

6.2. Effects of the Loss Function Choices

Setup. We explore the effect of the loss function on the robustness of a TTA method under RIP attack. Different choices of loss functions in Sec. 2.2: \mathcal{L}_{Ent} (Eq. 2), \mathcal{L}_{CE} (Eq. 3, augmentation), \mathcal{L}_{RMT} [6], and \mathcal{L}_{SLR} (Eq. 4) are used as \mathcal{L}_{CLS} in the baseline method’s update step (Eq. 6).

Results. Fig. 6c introduces the testing errors. The effect of RIP on each loss function choice is different. Notably, *all loss functions that involve augmented samples* (Eq. 5) as discussed in Sec. 2.2, such as \mathcal{L}_{CE} and \mathcal{L}_{RMT} , are more susceptible to RIP attack. In contrast, simpler loss functions like \mathcal{L}_{Ent} and \mathcal{L}_{SLR} perform well. \mathcal{L}_{RMT} , falling between these two categories of functions, is intermediate.

6.3. Effects of the Level of Augmentation

Setup. To confirm the suspicions of augmented samples, we investigate the correlation between the level of data augmentation and the tolerance of the baseline model to RIP. Following a prior study [49], random color jitter, affine transformations, and horizontal flipping are applied. The level of augmentation varies from 1 to 5 (5 is the strongest, and the typical level used in practice-[49]). Visit the Appendix for visual examples of these augmented samples.

Results. The effect of the RIP attack on the baseline algorithm is visualized in Fig. 6d. Unsurprisingly, *the damage of RIP is correlated with the level of augmentation used*, well explained by the shifting boundary effect in Sec. 3.2.

6.4. Effects of the Pseudo-label Predictor

Setup. Previous ablation studies identified the use of loss functions computed on augmented samples as the main cause of RIP vulnerability. Sec. 2.4 presents two choices of model for pseudo-label predictors: teacher (Eq. 9) and student (Eq. 10). They are investigated in this section.

Results. The experimental result in Fig. 6e shows that *the pseudo labels predicted by the student model make continual TTA methods more vulnerable to RIP attack, compared to the teacher model*. This can be explained by the improved accuracy of pseudo-labels for adaptation, as stated in [46].

6.5. Effects of the Model Update Rate

Setup. Extending the observation in Sec. 6.4, we study the effect of the update rate α (Eq. 7) on the resilience of the baseline model under RIP attack. Various values are chosen from $\alpha = 0$ (no mean teacher update) and $\alpha = 1$ (no TTA).

Results. Fig. 6f plots the testing error with increasing value of α . *The slower the update rate, the better the model can mitigate RIP attack*. However, it cannot be eliminated.

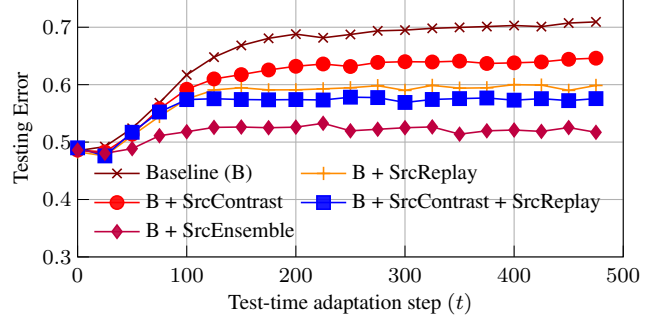


Figure 7. Average testing error of the baseline model (Sec. 6.1) with three simple RIP attack defensive attempts: source training replay (SrcReplay), contrastive loss with source prototypes (SrcContrast), and source model weight ensemble (SrcEnsemble).

7. Discussions and Conclusions

RIP Attack Defense. Although this is not the primary focus of this study, we still investigate some techniques: the source replay [6, 25], the contrastive loss [6, 20], and the source model weight ensemble (Eq. 8). Fig. 7 visualizes their effect. Constraining the model’s divergence from the source model appears to *help preserve the resistance* of the baseline TTA method, but it *does not fully eliminate the risk*. Eliminating Aug operator could remove the risk, but it comes at the cost of reduced performance. While using the teacher model for pseudo-label prediction can make the attack more difficult, there is a trade-off as noted in [39].

Limitations of RIP Attack. Though it may not be costly to execute, RIP attack still requires either collecting a small labeled dataset or a manual step to find incorrect predictions. From Sec. 5, 6, RIP attack can only succeed if a random augmentation operator is used. Although this is not a criterion in prior studies [2, 51], we recognize that these attempts, including RIP, require continuous sample submissions, occupying the testing stream for a prolonged period.

Future Work. The introduced RIP is relatively simple, only utilizing the final predicted label as the feedback signal for the attack purpose. An elaborated version of it can be developed by exploiting the output probability or the confidence score associated with each prediction. The ability to defend RIP attack is only briefly discussed, necessitating the development of an efficient RIP defense mechanism.

Conclusions. Orthogonal to prior TTA attack studies, *Reusing of Incorrect Prediction (RIP)* draws our attention to an untouched concern: “*Continual TTA is vulnerable to an intriguingly simple black-box algorithm*”. This study confirms the risk on recent continual TTA methods and highlights that the use of augmentation is correlated to RIP’s vulnerability. As the key mechanism, TTA makes a model more confident in their predictions after each adaptation step, which is undesirably, also magnifies the errors caused by incorrect pseudo-labels. This becomes a *backdoor* for attackers to intentionally collapse a continual TTA model.

References

- [1] Ahmed Aldahdooh, Wassim Hamidouche, Sid Ahmed Fezza, and Olivier Déforges. Adversarial example detection for DNN models: a review and experimental comparison. *Artificial Intelligence Review*, 55(6):4403–4462, 2022. 6
- [2] T. Cong, X. He, Y. Shen, and Y. Zhang. Test-time poisoning attacks against test-time adaptation models. In *IEEE Symposium on Security and Privacy (SP)*, pages 75–75, 2024. 1, 2, 5, 6, 8, 12
- [3] Francesco Croce, Maksym Andriushchenko, Vikash Sehwag, Edoardo Debenedetti, Nicolas Flammarion, Mung Chiang, Prateek Mittal, and Matthias Hein. Robust-bench: a standardized adversarial robustness benchmark. In *35th Conference on Neural Information Processing Systems (NeurIPS) Datasets and Benchmarks Track*, 2021. 14
- [4] Francesco Croce, Sven Gowal, Thomas Brunner, Evan Shelhamer, Matthias Hein, and Ali Taylan Cemgil. Evaluating the adversarial robustness of adaptive test-time defenses. In *Proceedings of the International Conference on Machine Learning (ICML)*, 2022. 12
- [5] Jia Deng, Wei Dong, Richard Socher, Li-Jia Li, Kai Li, and Li Fei-Fei. ImageNet: A large-scale hierarchical image database. In *IEEE Conference on Computer Vision and Pattern Recognition (CVPR)*, pages 248–255, 2009. 14
- [6] Mario Döbler, Robert A. Marsden, and Bin Yang. Robust mean teacher for continual and gradual test-time adaptation. In *Proceedings of the IEEE/CVF Conference on Computer Vision and Pattern Recognition (CVPR)*, pages 7704–7714, 2022. 2, 3, 6, 7, 8, 14
- [7] Yaroslav Ganin and Victor Lempitsky. Unsupervised domain adaptation by backpropagation. In *Proceedings of the 32nd International Conference on Machine Learning (ICML)*, pages 1180–1189, Lille, France, 2015. PMLR. 1
- [8] Taesik Gong, Jongheon Jeong, Taewon Kim, Yewon Kim, Jinwoo Shin, and Sung-Ju Lee. NOTE: Robust continual test-time adaptation against temporal correlation. In *Advances in Neural Information Processing Systems (NeurIPS)*, 2022. 1, 3, 6, 12
- [9] Ian J. Goodfellow, Jonathon Shlens, and Christian Szegedy. Explaining and harnessing adversarial examples. In *Proceedings of the 3rd International Conference on Learning Representations (ICLR)*, 2015. 1, 12
- [10] Sven Gowal, Sylvestre-Alvise Rebuffi, Olivia Wiles, Florian Stimberg, Dan Calian, and Timothy Mann. Improving robustness using generated data. In *35th International Conference on Neural Information Processing Systems (NeurIPS)*, 2021. 12
- [11] Yves Grandvalet and Yoshua Bengio. Semi-supervised learning by entropy minimization. In *Advances in Neural Information Processing Systems*, 2004. 3
- [12] Chuan Guo, Jacob Gardner, Yurong You, Andrew Gordon Wilson, and Kilian Weinberger. Simple black-box adversarial attacks. In *Proceedings of the 36th International Conference on Machine Learning (ICLR)*, pages 2484–2493. PMLR, 2019. 1
- [13] Kaiming He, Xiangyu Zhang, Shaoqing Ren, and Jian Sun. Deep residual learning for image recognition. *arXiv preprint arXiv:1512.03385*, 2015. 14
- [14] Dan Hendrycks and Thomas Dietterich. Benchmarking neural network robustness to common corruptions and perturbations. *Proceedings of the 7th International Conference on Learning Representations (ICLR)*, 2019. 3, 4, 6, 7, 8, 14
- [15] Dan Hendrycks, Norman Mu, Ekin D. Cubuk, Barret Zoph, Justin Gilmer, and Balaji Lakshminarayanan. AugMix: A simple data processing method to improve robustness and uncertainty. *Proceedings of the International Conference on Learning Representations (ICLR)*, 2020. 14
- [16] Dan Hendrycks, Steven Basart, Norman Mu, Saurav Kadavath, Frank Wang, Evan Dorundo, Rahul Desai, Tyler Zhu, Samyak Parajuli, Mike Guo, Dawn Song, Jacob Steinhardt, and Justin Gilmer. The many faces of robustness: A critical analysis of out-of-distribution generalization. In *Proceedings of the IEEE/CVF International Conference on Computer Vision (ICCV)*, pages 8320–8329, 2021. 2, 13
- [17] Trung-Hieu Hoang, Duc Minh Vo, and Minh N. Do. Persistent test-time adaptation in recurring testing scenarios. In *38th Annual Conference on Neural Information Processing Systems (NeurIPS)*, 2024. 1, 2, 3, 5, 6, 7, 12, 14
- [18] Trung-Hieu Hoang, Mona Zehni, Huy Phan, Duc Minh Vo, and Minh N. Do. Improving the robustness of 3D human pose estimation: A benchmark and learning from noisy input. In *Proceedings of the IEEE/CVF Conference on Computer Vision and Pattern Recognition (CVPR) Workshops*, pages 113–123, 2024. 1
- [19] Sergey Ioffe and Christian Szegedy. Batch Normalization: Accelerating deep network training by reducing internal covariate shift. In *Proceedings of the 32nd International Conference on Machine Learning (ICML)*, pages 448–456, Lille, France, 2015. PMLR. 8, 12, 14
- [20] Guoliang Kang, Lu Jiang, Yi Yang, and Alexander G Hauptmann. Contrastive adaptation network for unsupervised domain adaptation. In *Proceedings of the IEEE/CVF Conference on Computer Vision and Pattern Recognition (CVPR)*, pages 4893–4902, 2019. 8
- [21] Diederik P. Kingma and Jimmy Ba. Adam: A method for stochastic optimization. In *Proceedings of the 3rd International Conference on Learning Representations (ICLR)*, 2015. 14
- [22] Dong-Hyun Lee. Pseudo-label : The simple and efficient semi-supervised learning method for deep neural networks. *ICML 2013 Workshop : Challenges in Representation Learning (WREPL)*, 2013. 2
- [23] Bin Liang, Hongcheng Li, Miaoqiang Su, Xirong Li, Wenchang Shi, and Xiaofeng Wang. Detecting adversarial image examples in deep neural networks with adaptive noise reduction. *IEEE Transactions on Dependable and Secure Computing*, 18(1):72–85, 2021. 6, 12
- [24] Jian Liang, Dapeng Hu, and Jiashi Feng. Do we really need to access the source data? Source hypothesis transfer for unsupervised domain adaptation. In *Proceedings of the 37th International Conference on Machine Learning (ICML)*, pages 6028–6039, 2020. 12

- [25] Long-Ji Lin. Self-improving reactive agents based on reinforcement learning, planning and teaching. *Machine Learning*, 8(3–4):293–321, 1992. 8
- [26] Yuejiang Liu, Parth Kothari, Bastien van Delft, Baptiste Bellot-Gurlet, Taylor Mordan, and Alexandre Alahi. TTT++: When does self-supervised test-time training fail or thrive? In *Advances in Neural Information Processing Systems (NeurIPS)*, pages 21808–21820, 2021. 12
- [27] Alexander Lyzhov, Yuliya Molchanova, Arsenii Ashukha, Dmitry Molchanov, and Dmitry Vetrov. Greedy policy search: A simple baseline for learnable test-time augmentation. In *Proceedings of the 36th Conference on Uncertainty in Artificial Intelligence (UAI)*, pages 1308–1317. PMLR, 2020. 2
- [28] Aleksander Madry, Aleksandar Makelov, Ludwig Schmidt, Dimitris Tsipras, and Adrian Vladu. Towards deep learning models resistant to adversarial attacks. In *Proceedings of the 6th International Conference on Learning Representations (ICLR)*, 2018. 3
- [29] TorchVision maintainers and contributors. Torchvision: Pytorch’s computer vision library. <https://github.com/pytorch/vision>, 2016. 14
- [30] Robert A Marsden, Mario Döbler, and Bin Yang. Universal test-time adaptation through weight ensembling, diversity weighting, and prior correction. In *Proceedings of the IEEE/CVF Winter Conference on Applications of Computer Vision (WACV)*, pages 2555–2565, 2024. 3, 6, 7, 12
- [31] Chaithanya Kumar Mummadi, Robin Huttmacher, Kilian Rambach, Evgeny Levinkov, Thomas Brox, and Jan Hendrik Metzen. Test-time adaptation to distribution shift by confidence maximization and input transformation. *ArXiv*, abs/2106.14999, 2021. 3
- [32] Anh Nguyen, Jason Yosinski, and Jeff Clune. Deep neural networks are easily fooled: High confidence predictions for unrecognizable images. In *Proceedings of the IEEE/CVF Conference on Computer Vision and Pattern Recognition (CVPR)*, pages 427–436, 2015. 12
- [33] A. Tuan Nguyen, Thanh Nguyen-Tang, Ser-Nam Lim, and Philip Torr. TIPI: Test time adaptation with transformation invariance. In *Proceedings of the IEEE/CVF Conference on Computer Vision and Pattern Recognition (CVPR)*, 2023. 3, 12
- [34] Shuaicheng Niu, Jiayang Wu, Yifan Zhang, Yaofo Chen, Shijian Zheng, Peilin Zhao, and Mingkui Tan. Efficient test-time model adaptation without forgetting. In *Proceedings of the 39th International Conference on Machine Learning (ICML)*, 2022. 2, 6, 7, 12
- [35] Shuaicheng Niu, Jiayang Wu, Yifan Zhang, Zhiquan Wen, Yaofo Chen, Peilin Zhao, and Mingkui Tan. Towards stable test-time adaptation in dynamic wild world. In *Proceedings of the 17th International Conference on Learning Representations (ICLR)*, 2023. 12
- [36] Tianyu Pang, Chao Du, Yinpeng Dong, and Jun Zhu. Towards robust detection of adversarial examples. In *Advances in Neural Information Processing Systems (NeurIPS)*, 2018. 6, 12
- [37] Nicolas Papernot, Patrick McDaniel, Xi Wu, Somesh Jha, and Ananthram Swami. Distillation as a Defense to Adversarial Perturbations Against Deep Neural Networks. In *IEEE Symposium on Security and Privacy (SP)*, pages 582–597, 2016. 12
- [38] Nicolas Papernot, Patrick McDaniel, Ian Goodfellow, Somesh Jha, Z. Berkay Celik, and Ananthram Swami. Practical black-box attacks against machine learning. In *Proceedings of the 2017 ACM on Asia Conference on Computer and Communications Security*, page 506–519, New York, NY, USA, 2017. Association for Computing Machinery. 1, 5, 12
- [39] Hyejin Park, Jeongyeon Hwang, Sunung Mun, Sangdon Park, and Jungseul Ok. MedBN: Robust test-time adaptation against malicious test samples. In *Proceedings of the IEEE/CVF Conference on Computer Vision and Pattern Recognition (CVPR)*, pages 5997–6007, 2024. 1, 2, 6, 8, 12
- [40] Ori Press, Steffen Schneider, Matthias Kuehmerer, and Matthias Bethge. RDumb: A simple approach that questions our progress in continual test-time adaptation. In *37th Annual Conference on Neural Information Processing Systems (NeurIPS)*, 2023. 1, 12
- [41] Joaquin Quionero-Candela, Masashi Sugiyama, Anton Schwaighofer, and Neil D. Lawrence. *Dataset Shift in Machine Learning*. The MIT Press, 2009. 1, 2, 12
- [42] Connor Shorten and Taghi M Khoshgoftaar. A survey on image data augmentation for deep learning. *Journal of Big Data*, 6(1):1–48, 2019. 2
- [43] Yongyi Su, Xun Xu, and Kui Jia. Towards real-world test-time adaptation: Tri-Net self-training with balanced normalization. In *AAAI Conference on Artificial Intelligence*, 2023. 1, 3, 6, 7
- [44] Yu Sun, Xiaolong Wang, Zhuang Liu, John Miller, Alexei Efros, and Moritz Hardt. Test-time training with self-supervision for generalization under distribution shifts. In *Proceedings of the 37th International Conference on Machine Learning (ICML)*, pages 9229–9248. PMLR, 2020. 12
- [45] Christian Szegedy, Wojciech Zaremba, Ilya Sutskever, Joan Bruna, Dumitru Erhan, Ian J. Goodfellow, and Rob Fergus. Intriguing properties of neural networks. In *Proceedings of the 2nd International Conference on Learning Representations (ICLR)*, 2014. 1, 12
- [46] Antti Tarvainen and Harri Valpola. Mean teachers are better role models: Weight-averaged consistency targets improve semi-supervised deep learning results. In *31st International Conference on Neural Information Processing Systems (NeurIPS)*, page 1195–1204, 2017. 3, 8, 12
- [47] Laurens van der Maaten and Geoffrey Hinton. Visualizing data using t-SNE. *Journal of Machine Learning Research (JMLR)*, 9(86):2579–2605, 2008. 3, 4
- [48] Dequan Wang, Evan Shelhamer, Shaoteng Liu, Bruno Olshausen, and Trevor Darrell. Tent: Fully test-time adaptation by entropy minimization. In *Proceedings of the 9th International Conference on Learning Representations (ICLR)*, 2021. 1, 2, 3, 8, 12, 14
- [49] Qin Wang, Olga Fink, Luc Van Gool, and Dengxin Dai. Continual test-time domain adaptation. In *Proceedings of the IEEE/CVF Conference on Computer Vision and Pattern Recognition (CVPR)*, pages 7201–7211, 2022. 1, 2, 3, 6, 7, 8, 12, 14

- [50] Yulong Wang, Tong Sun, Shenghong Li, Xin Yuan, Wei Ni, Ekram Hossain, and H. Vincent Poor. Adversarial attacks and defenses in machine learning-empowered communication systems and networks: A contemporary survey. *IEEE Communications Surveys and Tutorials*, 25(4):2245–2298, 2023. [1](#), [6](#), [12](#)
- [51] Tong Wu, Feiran Jia, Xiangyu Qi, Jiachen T. Wang, Vikash Sehwal, Saeed Mahlouljifar, and Prateek Mittal. Uncovering adversarial risks of test-time adaptation. In *Proceedings of the 40th International Conference on Machine Learning (ICML)*. JMLR.org, 2023. [1](#), [2](#), [5](#), [6](#), [8](#), [12](#)
- [52] Ying Xu, Xu Zhong, Antonio Jimeno Yepes, and Jey Han Lau. Grey-box adversarial attack and defence for sentiment classification. In *Proceedings of the 2021 Conference of the North American Chapter of the Association for Computational Linguistics: Human Language Technologies*, pages 4078–4087, Online, 2021. Association for Computational Linguistics. [12](#)
- [53] Longhui Yuan, Binhui Xie, and Shuang Li. Robust test-time adaptation in dynamic scenarios. In *Proceedings of the IEEE/CVF Conference on Computer Vision and Pattern Recognition (CVPR)*, pages 15922–15932, 2023. [1](#), [2](#), [3](#), [6](#), [7](#), [12](#), [14](#)
- [54] Hongyi Zhang, Moustapha Cisse, Yann N. Dauphin, and David Lopez-Paz. mixup: Beyond empirical risk minimization. In *Proceedings of the 6th International Conference on Learning Representations (ICLR)*, 2018. [3](#)
- [55] Marvin Zhang, Sergey Levine, and Chelsea Finn. MEMO: Test time robustness via adaptation and augmentation. In *36th Annual Conference on Neural Information Processing Systems (NeurIPS)*, pages 38629–38642, 2022. [2](#)
- [56] Kaiyang Zhou, Ziwei Liu, Yu Qiao, Tao Xiang, and Chen Change Loy. Domain generalization: A survey. *IEEE Transaction on Pattern Analysis and Machine Intelligence (TPAMI)*, 45(4):4396–4415, 2023. [12](#)

R.I.P. : A Simple Black-box Attack on Continual Test-time Adaptation

Supplementary Material

A. Related Work

Continual Test-time Adaptation (TTA). Under the circumstance of testing data distribution diverged [41], *Test-Time Adaptation (TTA)*, a domain generalization technique [56], enhances the performance of a machine learning (ML) model by enabling its parameters to change through test-time training [26, 44]. Fundamentally, TTA encourages the ML model to be more confident in their predictions by minimizing the prediction entropy [24, 33–35, 48, 48]. Observing that the distribution may not happen once, but can be changed continuously, later studies extend the TTA approach to multiple shifts setting [17, 40, 49]. Towards real-world TTA, recent research studies TTA also investigate the scenarios where the label distribution is non-i.i.d., or temporally correlated [8, 30, 35, 53]. These studies, on the one hand, address major failure modes of TTA on challenging testing streams, are far more complicated than earlier methods such as [34, 49]. This necessitates further investigation into their reliability and trustworthiness during deployment, *with RIP attacks being on this line of inquiry.*

Adversarial Attacks and Defenses in ML. An adversarial attack aims to degrade the performance of a victim ML model by manipulating the input data, causing it to produce false predictions [9, 32, 45, 50]. Those attempts can be classified into main categories: white-box, black-box, and gray-box [52], based on the attacker’s knowledge of the victim system. The white-box attack assumes the model is fully accessible, allowing gradient-based algorithms to craft the adversarial samples [9, 45]. Meanwhile, the black-box attack strictly restricts these favors and repetitively queries the model to adjust the strategy [38]. *A black-box attack is significantly more realistic.* Adversarial defense techniques are also explored to counteract attack attempts. Straightforwardly, a trained ML model to detect and filter adversarial samples [23, 36, 50]. More advanced techniques can make the model more robust to such perturbations during training [10, 37] or be more adaptive at test time [4].

Continual TTA Attack. While adversarial attack and continual TTA are two active research areas, only a limited number of prior studies investigate this risk on continual TTA methods. Poisoning [2] or distribution invading [39, 51] attacks are among the first studies uncovering the risk of continual TTA being manipulated by injecting malicious testing samples. Even though they are the closest to our work, both fall into the *white-box attack category* that assumes the attacker has complete knowledge of the underlying model. In contrast, our RIP attack neither makes any assumptions about the operating TTA algorithm nor the

adaptation process, and we simply audit the model outputs to modify the attack scheme. To the best of our knowledge, *we are the first to introduce an implementable black-box attack algorithm targeting a continual TTA method.*

Comparison of RIP Versus Previous Continual TTA Attack Studies. Besides studying a black-box continual TTA attack for the first time, *this work is orthogonal to the prior studies [2, 39, 51] in multiple aspects.* Firstly, the investigation here primarily focuses on the risk during self-training (data augmentation, loss function, model update, and pseudo-label predictor) utilized for the TTA process, not the risk in intercepting the batch normalization [19] statistics like [39, 51] to create false predictions. The long-term effect on a TTA model after the attack is not also well investigated. Secondly, this work targets the recent *continual* TTA algorithms, mean-teacher model update [46], not the traditional single-domain TTA approaches [33, 35, 48]. Thirdly, the attack action of RIP is inherently natural, as it simply reuses images from the testing distribution without requiring any image-level modifications via adversarial training and gradient descent update [9, 45].

B. Additional RIP Attack Results

In Alg. 1, all the input parameters of RIP attack have been introduced. Within the main text, the effectiveness of RIP has been demonstrated on a variety of different continual TTA methods (varying $f_t(x)$) (Sec. 5.2). While the number of attack steps T_a can be monitored by determining whether the model performance is saturated, this section provides additional RIP attack results to complete the discussion. Specifically, we study RIP attack with varying victim class y_a (Sec. B.1), labeled attack dataset \mathcal{D}_a (Sec. B.2) and testing batch size B (Sec. B.3).

B.1. Varying Victim Classes

We provide the confusion matrices of the baseline continual TTA method (Sec. 6.1) under RIP attack in Fig. 8. Here, the confusion matrix of this model at the 1st, 100th, and the 400th adaptation step is visualized. From this figure, we can see the effect of RIP attack with *three different choices of the victim class y_a .* It is hard to see in the main tables and figures since they provide the averaged value across all 10 selected classes (or trials, as defined in the main text). Nevertheless, the observation is similar, regardless of the selected victim class. Furthermore, this figure also showcases the “*shifting boundary effect*” (Fig. 4 and Sec. 3.2) on a real image dataset. A transition in the model predictions on the victim class to the most misclassified class is consistently observed in all the choices of the victim class.

B.2. Varying Choices of Labeled Attack Dataset

RIP attack requires a dataset with labels \mathcal{D}_a to perform (for checking the correctness of the model predictions). In

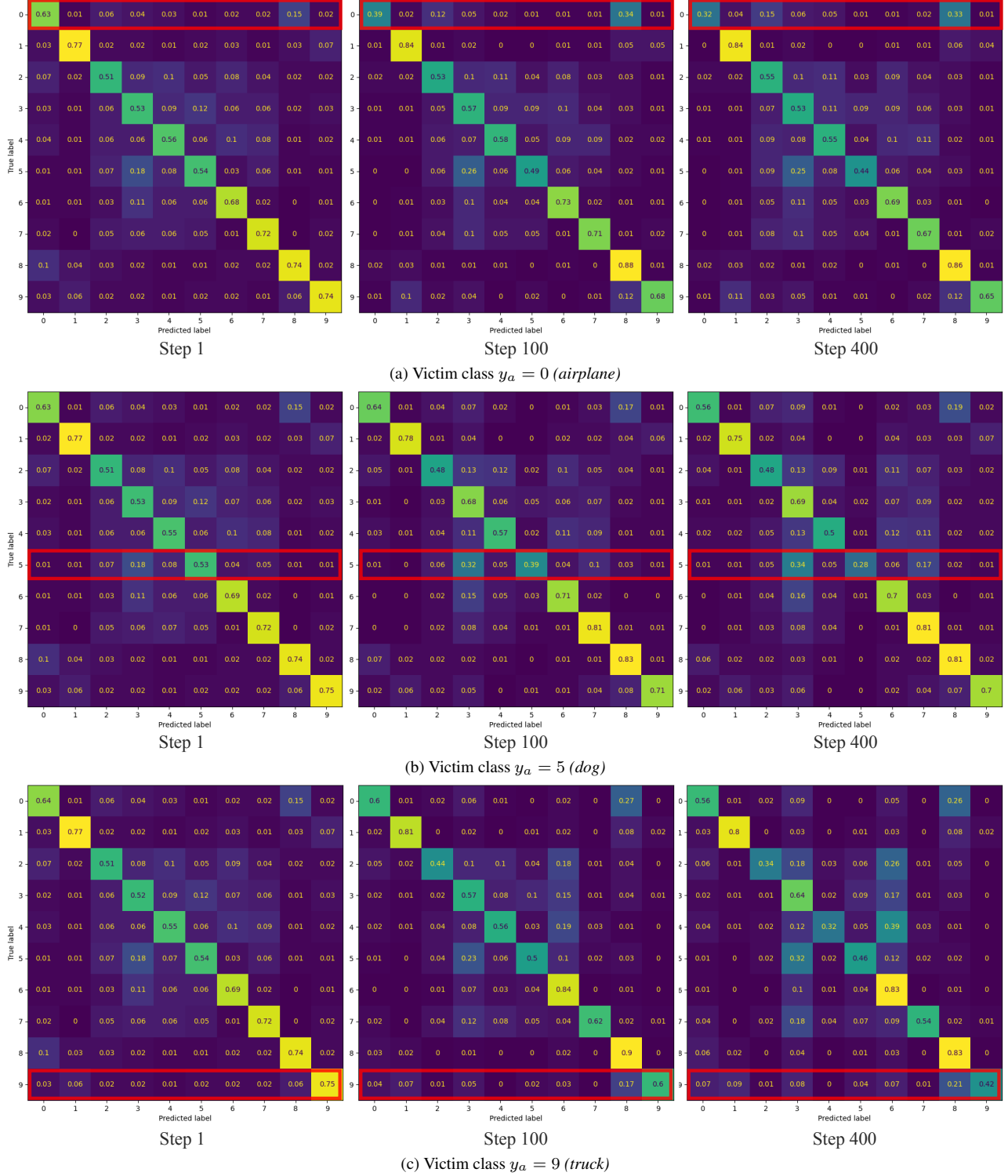
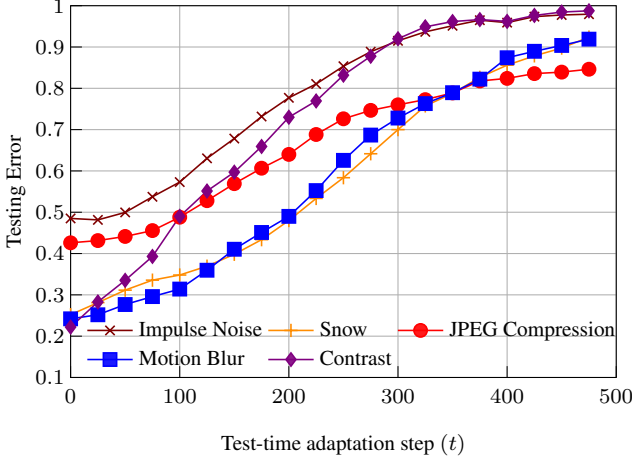
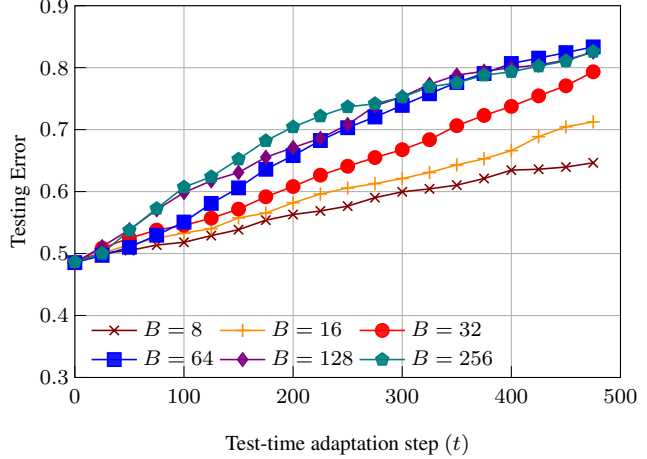


Figure 8. Confusion matrices under RIP attack of the baseline continual TTA method (Sec. 6.1) at the 1st, 100th and the 400th step. CIFAR-10-C [16] is used with three choices of victim class: (a) $y_a = 0$ (airplane), (b) $y_a = 5$ (dog), and (c) $y_a = 9$ (truck) for demonstration, the other classes follow similarly. The rows presenting the true labels are highlighted in red boxes. We direct readers' attention to the victim class and the entry in this row most susceptible to misclassification. As adaptation proceeds, the model increasingly tends to further misclassify this entry as the victim class. This observation agrees with the *shifting boundary effect* (Fig. 4 and Sec. 3.2).



(a) Various choices of the attack dataset \mathcal{D}_a .



(b) Various choices of the testing batch size B .

Figure 9. Average testing error of the baseline model (Sec. 6.1) with different variations of RIP attack.

the main experiments on CIFAR-10C, CIFAR-100-C, and ImageNet-C [14], we conveniently adopt the set of impulse-noise corrupted images (at level 5) from these datasets. We note that this choice of corruption is arbitrary, and one can generate a similar dataset as long as there is a distribution mismatch with the source model, and it is likely to produce incorrect predictions. In Fig. 9a, we present the baseline model collapsed by 4 other choices of \mathcal{D}_a , formed by picking other types of corruptions: snow, JPEG compression, motion blur, and contrast adjustment. They are representatives for their group, among a total of 15 corruptions in [14]. We observe a similar collapse pattern on the baseline model regardless of the choice of \mathcal{D}_a .

B.3. Varying Choices of Testing Batch Size

We use a batch size of $B = 64$, following previous studies [6, 49, 53] in our main experiments. In Fig. 9b, we further investigate RIP attack on the baseline model with varying choices of $B \in \{8, 16, 32, 64, 128, 256\}$. RIP attack consistently increases testing error across all choices of B , though the amount may vary with a larger batch size favors the attack. The effect of increasing batch size seems saturated for the choices larger than 64.

C. Implementation Details

C.1. Random Data Augmentation Operator

Following prior work [49], the image-level data augmentation $\text{Aug}(\cdot)$ investigated in this study is composed of a series of operators: *random horizontal flipping*, *affine transformation*, *color jittering*, *additive Gaussian noise*, *blurring by a Gaussian kernel*. Sec. 6.3 introduces five level of augmentations. They are created by varying the degree of ran-

domness and the strength of each component augmentation operator. Specifically, we keep the probability for random horizontal flipping at 0.5 and the kernel size of 3, standard deviation of 0.005 for the Gaussian blur at all levels. Other components' parameters at each level are detailed in Tab. 3.

For illustration, in Fig. 10, the effect of augmentation on an image in ImageNet [5] at each level is provided.

C.2. The Numerical Simulation on Gaussian Mixture Model Classifier (GMMC)

For the GMMC simulation mentioned in our analysis, a toy dataset is constructed with $N = 1,000$ data points, drawn from a mixture of two Gaussian distributions: $(\mu_0, \mu_1) = (-1.0, 2.0)$ and $\sigma_0 = \sigma_1 = 1.0$. We simulate a TTA process with $T_a = 120$ steps. The level of augmentation in the Additive White Gaussian Noise (AWGN) operator is set to $\sigma = 0.2$. Visit [17] for further discussions on GMMC.

C.3. Continual Test-time Adaptation Methods

Source Model and Dataset. RobustBench [3] and torchvision [29] provide the initial models (f_0) trained on the source distributions. From RobustBench, the model with checkpoint Standard and Hendrycks2020AugMix_ResNeXt [15] are adopted for CIFAR10-C and CIFAR-100-C experiments, respectively. The ResNet50 [13] model pre-trained on ImageNet V2 (specifically, checkpoint ResNet50_Weights.IMAGENET1K_V2 of torchvision) is used for ImageNet-C experiments.

Updated Parameters. Following prior studies [6, 48, 49, 53], θ_t - the linear parameters of batch norm layers [19] are updated at each adaptation step t .

Optimizer. Adam [21] optimizer with learning rate equal



Figure 10. An example of augmented images at five different data augmentation levels.

Level	Gaussian Noise	Random Affine		Color Jitter				
		Degrees	Scale	Brightness	Contrast	Saturation	Hue	Gamma
1	$\sigma \in [0, 001, 0.05]$	$[-1, 1]$	$[0.95, 0.97]$	$[0.85, 0.87]$	$[0.85, 0.90]$	$[0.75, 0.80]$	$[-0.005, 0.005]$	$[0.95, 1.00]$
2	$\sigma \in [0, 001, 0.10]$	$[-2, 2]$	$[0.95, 1.00]$	$[0.8, 0.9]$	$[0.85, 0.95]$	$[0.75, 0.85]$	$[-0.01, 0.01]$	$[0.95, 1.05]$
3	$\sigma \in [0, 001, 0.15]$	$[-4, 4]$	$[0.95, 1.05]$	$[0.9, 1.1]$	$[0.85, 1.05]$	$[0.75, 1.15]$	$[-0.02, 0.02]$	$[0.85, 1.05]$
4	$\sigma \in [0, 001, 0.15]$	$[-8, 8]$	$[0.95, 1.05]$	$[0.8, 1.2]$	$[0.85, 1.15]$	$[0.75, 1.25]$	$[-0.03, 0.03]$	$[0.85, 1.05]$
5	$\sigma \in [0, 001, 0.25]$	$[-15, 15]$	$[0.9, 1.1]$	$[0.6, 1.4]$	$[0.7, 1.3]$	$[0.50, 1.50]$	$[-0.06, 0.06]$	$[0.7, 1.3]$

Table 3. Parameters for the component random data augmentation operators in Aug at five different levels.

$1e^{-3}$, and $\beta = (0.9, 0.999)$ is selected as a universal choice for all experiments.

C.4. RIP Attack Trials

As mentioned in the experimental setup, the average performance across 10 RIP attack trials is reported. For each trial, all settings are kept the same, except for the victim class y_a . This class is uniformly sampled without replacement from all possible classes. For reproducibility, we list the index of the victim classes (y_a) used in our experiments:

- CIFAR-10-C: 0, 1, 2, 3, 4, 5, 6, 7, 8, 9, 10 (*all classes*).
- CIFAR-100-C: 3, 8, 29, 48, 56, 67, 71, 88, 91, 96.
- ImageNet-C: 91, 323, 392, 583, 630, 637, 643, 707, 864, 952.

C.5. Computing Resources

Experiments are conducted on a computer cluster with an Intel(R) Core(TM) 3.30GHz Intel Core i9-9820X CPU, 128 GB RAM, and 4×NVIDIA Quadro RTX 5000 GPUs.